Journal of Engineering Mathematics **41:** 305–327, 2001.

Wellbore stresses induced by the nonlinear deformation of an inflatable packer

C. ATKINSON[1], J. DESROCHES[2], D. A. EFTAXIOPOULOS[3] and M. THIERCELIN[4]
[1]*Department of Mathematics, Imperial College of Science, Technology and Medicine, 180 Queen's Gate, London SW7 2BZ, U.K.*
[2]*Schlumberger Dowell, 110 Schlumberger Drive, MD#2, Sugar Land, TX 7077, U.S.A.*
[3]*Department of Mechanics, Faculty of Applied Sciences, National Technical University of Athens, Zografou Campus, GR-15773 Athens, Greece*
[4]*Schlumberger Dowell, 26 rue de la Cavee, B.P. 202, 92142 Clamart, France*

Received 10 April 2000; accepted in revised form 28 March 2001

Abstract. Packers, *i.e.* inflatable balloons made from elastomere, reinforced with cords, are used by the oil industry for sealing an interval along the wellbore, for open – hole stress tests to be performed. Thiercelin *et al.* have shown that the packer behaviour is critical to the success of such tests. In particular, the pressure exerted by the packer on the formation needs to be as close as possible to the pressure in the interval, to avoid fracture initiation or fracture growth along the packers. Moreover, axial tension in the rock needs to be kept to a minimum to avoid initiation of transverse fractures at the packer level that would be detrimental to the test. In this paper the theory of membranes, reinforced with inextensible cords, developed by Kydoniefs and its implementation for packers done by Atkinson and Peltier, is used to gain insight into the stresses which are generated in the rock, due to packer inflation. The shape of the packer is first computed for a given net pressure across the packer, via the solution of a nonlinear integral equation. Then the pressure acting on the formation, along the packer/rock contact zone, is found. Results show that the pressure applied by the packer on the rock during stress testing, is almost uniform and close to packer inflation pressure. The formation is afterwards considered loaded with the latter pressure and the stresses in the rock are found by either a finite-element or a semi-analytic method. Axial stresses develop at packer ends but are much smaller than the pressure applied to the formation. Tangential stresses develop at the wellbore wall and are higher at packer level than at interval level.

Key words: inflatable packer, nonlinear deformation, wellbore stress.

1. Introduction

The Dual Packer Module (MRPA*) of the Modular Formation Dynamics Tester (MDT*) is used to perform open-hole stress tests. Previous research by Thiercelin *et al.* [1] has revealed that the packer behaviour is critical to the success of such tests. In particular, the pressure exerted by the packer on the formation needs to be as close as possible to the pressure in the interval to avoid fracture initiation or fracture growth along the packers. Moreover, axial tension in the rock needs to be kept to a minimum to avoid initiation of transverse fractures at the packer level that would be detrimental to the test.

This paper presents the use of a packer model to gain insight into the stresses which are generated at the wellbore wall by the packer inflation. The packer model that we consider in this paper consists of an inflatable, reinforced and initially cylindrical membrane. The reinforcing consists of two families of inextensible cords. This corresponds to the sliding coupling

*Mark of Schlumberger.

mechanism that the MRPA elements have. Although these elements consist of several layers with different properties, it has been shown in [4] that their behaviour is dominated by the properties of the main reinforcing layer. The model presented here is therefore meaningful, although the results will have to remain qualitative.

Kydoniefs [2] has developed the theory for the axisymmetric deformation of an initially cylindrical membrane, composed of an elastic, homogeneous, isotropic and incompressible material, possessing a general strain energy function and reinforced by two families of perfectly flexible and inextensible helicoidal cords. He also gave applications to specific boundary-value problems. The theory developed by Kydoniefs [2], was implemented by Atkinson and Peltier [3], in the case of a packer membrane reinforced with inextensible cords. They presented results for the deformed shape of the packer, the tension in the cords and the shear stress and strain in the membrane. Based on the output of their model, they made packer design suggestions that could be of practical significance.

In this paper we use the theory developed by Kydoniefs [2] and the methods implemented by Atkinson and Peltier [3], in order to evaluate the pressure exerted by inflatable packers, on the wellbore. A single packer and a straddle packer arrangement (two packers one below the other) are considered. The borehole is considered as rigid, as long as the packer shape is to be found. A justification of this assumption is given, by showing that the radial displacement on the open hole wall due to packer pressure is very small and does not alter the touch pressure and consequently the pressure profile as well. Two extremes are considered for the interface between the packer and the wellbore wall: a perfect slip (zero shear stress) or a perfect bond (zero axial displacement) condition. It, however, turns out that the for both packer/wellbore interface conditions, the very same packer shape is yielded, within a constant due to the different position of the point, which the initial mid point of the packer in the undeformed configuration, is mapped to. For large net pressures, *i.e.*, much greater than touch pressures, the packer shape remains unaltered when the net pressure is changed.

Once the packer shape has been computed, the pressure profile acting on the formation, along the contact zone between the packer and the wellbore, is found via the solution of a nonlinear integral equation. Still the formation is considered rigid, and the pressure profile along the packer/wellbore interface is yielded as almost uniform.

Having found the pressure profile acting on the borehole due to the inflated packer, we then evaluate the stresses that are generated in the rock, due to a single packer. The rock is now considered as an elastic material, loaded axisymmetrically by the packer induced pressure. Pure bond and pure slip packer/formation interface conditions are again considered. Two approaches, a finite element one and a semi-analytic one are followed for the determination of the stresses into the rock. Both give almost identical results. The value of the axial stress σ_{zz} is, for both pure bond and pure slip cases, significantly smaller than the radial and tangential stresses. However, the maximum positive σ_{zz} for the perfect slip case is almost three times larger than σ_{zz} for the perfect bond case.

Another important result, which is a consequence of the small value of the touch pressure, is the confirmation that the tangential stress $\sigma_{\theta\theta}$ at the wellbore wall is close to packer pressure. This implies that during a sleeve fracturing operation, (*i.e.*, initiation of a fracture by applying pressure on the wellbore while preventing the fluid from entering the rock by the use of a sleeve), creation of an axial fracture along the entire contact length is much more likely than creation of a transverse fracture.

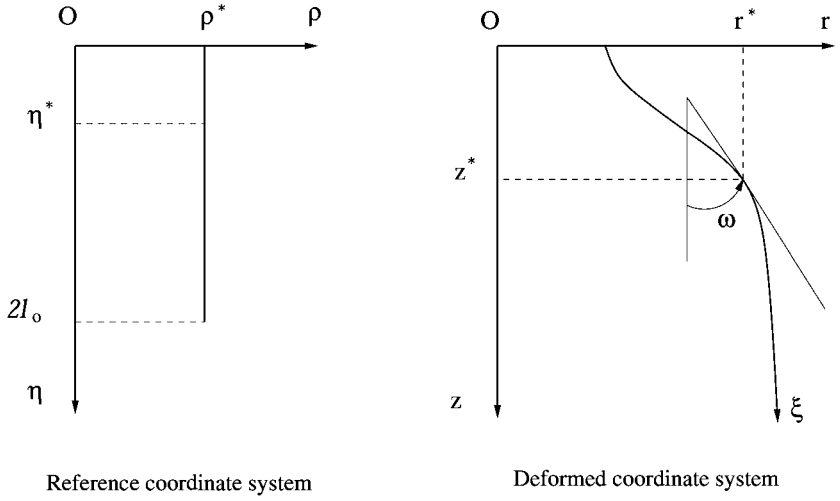

Figure 1. Framework for the analysis.

2. The shape of the packer membrane

Inflatable packers are considered as initially cylindrical membranes of length $2l_0$ and uniform thickness $2h_0$, composed of an elastic, homogeneous, isotropic and incompressible material, possessing a strain energy function $W = W(I_1, I_2)$ and reinforced by two families of perfectly flexible and inextensible cords. The model used in this paper for the simulation of the deformation of inflatable packers, is the one developed by Kydoniefs [2]. The same model was also used by Atkinson and Peltier [3] in their study of the levels of strain and stress in the membrane and the cords within a packer. For a detailed account of the underlying theory, the reader should resource to [2] and [3].

For a brief account of the geometry of the problem, Figure 1 is invoked. The deformation is referred to two systems of cylindrical coordinates, namely (O, ρ, θ, η) for the undeformed configuration and (O, r, θ, z) for the deformed configuration (Figure 1). The point of origin O is taken so that η and z are measured from the top (fixed) part of the packer membrane and are positive downwards. $(\rho^*, \theta^*, \eta^*)$, with $\rho^* = constant$, are then the coordinates in the undeformed configuration, of a point which has coordinates (r^*, θ^*, z^*) in the deformed state.

An expression for the strain energy density of the elastomer of the packer, has been deduced from experimental tests [4]. A representative, in SI units, is

$$W = 0{\cdot}24 \times 10^6(I_1 - 3) + 0{\cdot}0084 \times 10^6(I_1 - 3)^2. \tag{1}$$

Using this expression, we can deduce the functions of the forces in the elastomere, which then allows the computation of the angle ω (see [2] and [3]).

The shape of the packer membrane is computed for either the perfect slip (zero shear stress) or the perfect bond (zero axial displacement) condition, between the packer membrane and the wellbore wall. Any real situation is bound to lie between these two limiting cases. For each one of the above cases, two subcases are considered: either the membrane touches the wellbore wall at a single point, or the membrane is in contact with the wellbore wall over a finite length. In all cases, the maximum expansion ratio Λ_2 is given by:

$$\Lambda_2 = \frac{R_w}{\rho}, \tag{2}$$

where R_w is the wellbore radius.

When the membrane touches the wall at a single point, the shape of the free membrane and the value of the net pressure are solved for; in the case where the membrane is in contact with the wellbore wall over a finite length, the net pressure is given, and the shape of the free membrane together with the extension of the contact length are solved for. Note that a reasoning similar to that when the membrane touches the wall at a single point, could be used to determine the shape of the membrane when it does not touch the wellbore wall at all, with Λ_2 different from R_w/ρ.

Considering the two systems of reference shown in Figure 1, we see that the use of large deformations implies the following relations between the deformed shape and the undeformed (reference) shape:

$$\frac{\mathrm{d}z}{\mathrm{d}r} = \cot(\omega), \quad \frac{\mathrm{d}r}{\mathrm{d}\xi} = \sin(\omega), \quad \mathrm{d}r = \rho \mathrm{d}\lambda_2, \quad \mathrm{d}\eta = \frac{\mathrm{d}\xi}{\lambda_1}. \tag{3}$$

These expressions will be used to determine the complete shape of the packer in the following subsections.

If one considers a point X defined by (ρ, η) in the reference system and mapped to (r, z) in the deformed system, Equations (3) yield the following relationships:

$$\lambda_2 = \frac{r}{\rho}, \tag{4}$$

$$z = \rho \int \cot(\omega)\, \mathrm{d}\lambda_2, \tag{5}$$

$$\eta = \rho \int \frac{\mathrm{d}\lambda_2}{\lambda_1 \sin(\omega)}, \tag{6}$$

$$\xi = \rho \int \frac{\mathrm{d}\lambda_2}{\sin(\omega)}. \tag{7}$$

Note that the limits of the above integrals will depend on the choice of origin and orientation of z and η.

2.1. Perfect slip between the packer and the formation

In this case we assume that the rock/packer interface is free to slip, which means that, along the interface, $\tau_{r\theta} = \tau_{rz} = 0$.

2.1.1. *The net pressure in the packer is equal to the touch pressure*

Let us call net pressure the value of the pressure acting across the membrane, *i.e.*, the difference between the pressure in the packer P_k and the hydrostatic pressure P_h. In this case, the pressure in the packer P_k is such that the membrane does touch the wall at a single point B, which happens to be in the middle of the packer. The corresponding value of the net pressure is called touch pressure P_o.

Figure 2a shows the membrane in the current configuration and the reference configuration. The points A', C' as well as the middle point B' map into the points A, C and B, respectively, through the deformation. Note that $\omega(P)$, which denotes the angle formed by the tangent to the meridian of the deformed membrane and the axis of symmetry, is a function of the

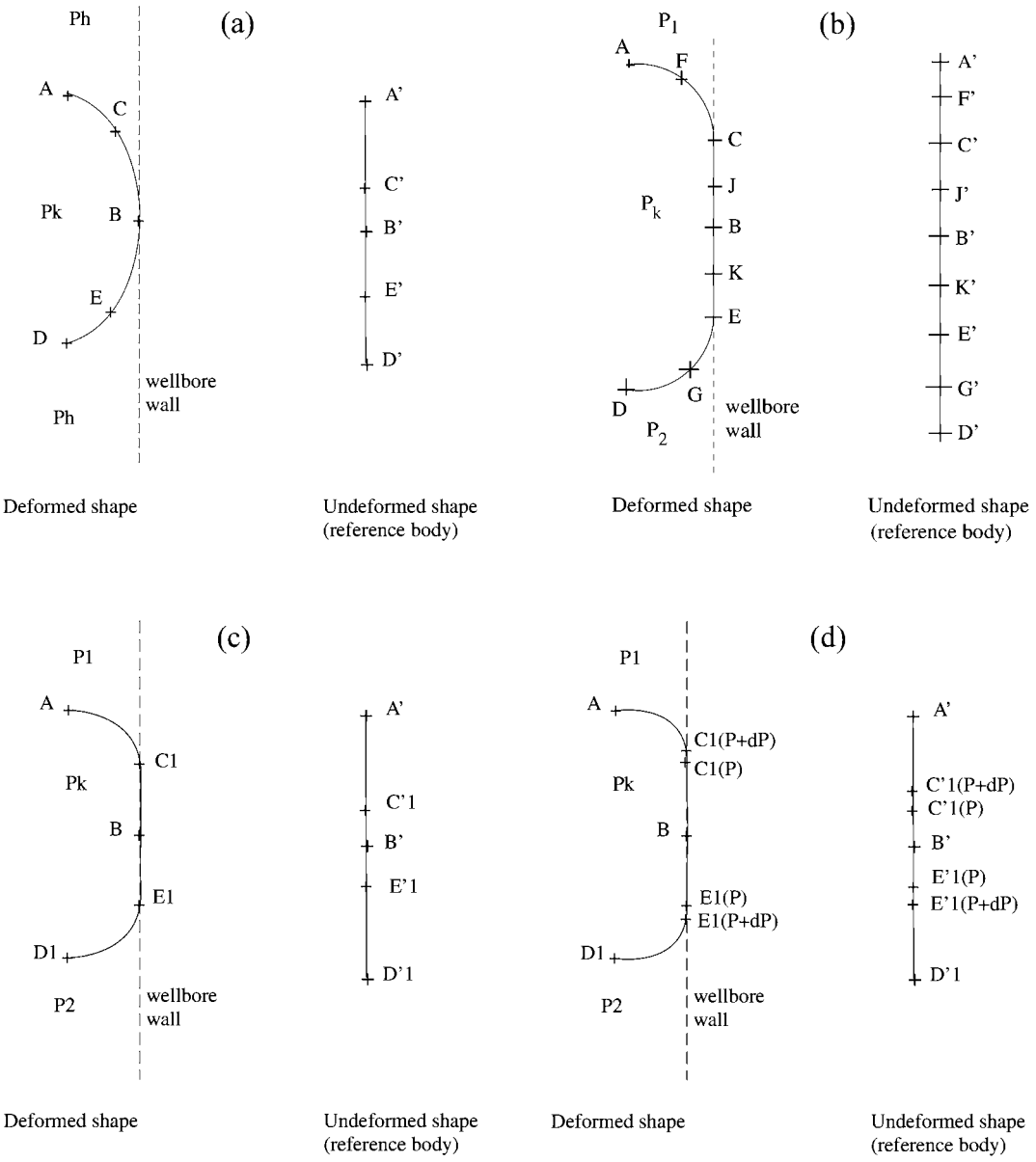

Figure 2. Shape of the membrane in the deformed and undeformed configurations. (a) Schematic diagram of a meridian of the packer membrane at touch pressure. (b) Shape of the meridian for a pressure greater than touch pressure. (c) Shape of the membrane for the no-slip case. (d) Shape of the membrane for the no-slip case for a pressure increment.

pressure P. Equation (24) in [3] relates ω with P. The appropriate theory for the derivation of Equation (24) in [3] is also presented in [3].

At touch pressure, the mapping between the deformed shape and the undeformed shape yields:

$$A'B' = B'D' = \rho \int_1^{\Lambda_2} \frac{\mathrm{d}\lambda_2}{\lambda_1 \sin \omega(P_o)} = l_o \tag{8}$$

and $\Lambda_2 = R_w/\rho$, where R_w is the wellbore radius and ρ the initial radius of the packer membrane. The value of the touch pressure P_o is determined by solving this nonlinear integral equation, for example by an iterative method.

Once the value of P_o has been computed, the complete shape of the packer membrane can be determined with z being a function of r:

$$z_A = 0, \tag{9}$$

$$z_C(r) = \rho \int_1^{\lambda_2^*} \cot(\omega(P_o))\, \mathrm{d}\lambda_2, \tag{10}$$

$$\lambda_2^* = r/\rho, \quad z_B = \rho \int_1^{\Lambda_2} \cot(\omega(P_o))\, \mathrm{d}\lambda_2, \tag{11}$$

$$z_E(r) = \rho \int_1^{\Lambda_2} \cot(\omega(P_o))\, \mathrm{d}\lambda_2 - \rho \int_{\Lambda_2}^{\lambda_2^*} \cot(\omega(P_o))\, \mathrm{d}\lambda_2, \tag{12}$$

$$z_D = 2\rho \int_1^{\Lambda_2} \cot(\omega(P_o))\, \mathrm{d}\lambda_2. \tag{13}$$

2.1.2. *The net pressure in the packer is above touch pressure*

As the packer pressure is increased, the current configuration looks as shown in Figure 2b. Under this configuration the point B may have moved (up) compared to the previous configurations. The pressure in the packer is P_k. The packer is now sealing, and the pressure P_1, above the packer, is not necessarily equal to the pressure P_2 below the packer. If the top packer of a straddle-packer arrangement is considered, P_2 is the pressure in the test interval and P_1 is the pressure in the remainder of the well, whereas it is the reverse if the bottom packer of such an arrangement is considered. AC has therefore the pressure $P_{AC} = P_k - P_1$ acting across it and DE has the pressure $P_{DE} = P_k - P_2$ acting across it.

Note that both Λ_2 and the values of the net pressure across both halves of the packer are now known, which leaves only the shape of the packer to be determined.

Note that $A'D' = 2l_o$, which is the length of the packer membrane in the reference body, is fixed. Then:

$$Z_C = \rho \int_1^{\Lambda_2} \cot(\omega(P_{AC}))\, \mathrm{d}\lambda_2, \tag{14}$$

$$Z_A = 0, \tag{15}$$

$$Z_B = Z_C + (C'B')\Lambda_1, \tag{16}$$

$$Z_E = Z_B + (B'E')\Lambda_1, \tag{17}$$

$$Z_D = Z_E + \rho \int_1^{\Lambda_2} \cot(\omega(P_{DE}))\, \mathrm{d}\lambda_2. \tag{18}$$

Now:

$$A'C' = \rho \int_1^{\Lambda_2} \frac{\mathrm{d}\lambda_2}{\lambda_1 \sin \omega(P_{AC})}, \tag{19}$$

$$E'D' = \rho \int_1^{\Lambda_2} \frac{d\lambda_2}{\lambda_1 \sin \omega(P_{DE})} \tag{20}$$

and

$$C'E' = 2l_o - A'C' - E'D'. \tag{21}$$

So we can miss out Z_B (Equation 16) since $Z_E = Z_C + (C'E')\Lambda_1$ and the point B will presumably have moved. We know that $A'B' = l_o$ so:

$$Z_B = Z_C + \Lambda_1(l_o - A'C') \tag{22}$$

Putting everything together, we can now determine the complete deformed shape of the packer. For a point F located between A and C (Figure 2b) we have:

$$Z_{F=A} = 0, \tag{23}$$

$$Z_F(\lambda_2^*) = \rho \int_1^{\lambda_2^*} \cot(\omega(P_{AC}))\, d\lambda_2 \tag{24}$$

with $\lambda_2^* = r/\rho$

$$Z_{F=C} = \rho \int_1^{\Lambda_2} \cot(\omega(P_{AC}))d\lambda_2 \tag{25}$$

and for a point G located between E and D (Figure 2b):

$$Z_{G=E} = Z_C + 2\Lambda_1 l_o - \Lambda_1 \rho \int_1^{\Lambda_2} [\frac{1}{\lambda_1 \sin \omega(P_{AC})} + \frac{1}{\lambda_1 \sin \omega(P_{DE})}]\, d\lambda_2, \tag{26}$$

$$Z_G(\lambda_2^*) = Z_E + \rho \int_{\lambda_2^*}^{\Lambda_2} \cot \omega(P_{DE})d\lambda_2, \tag{27}$$

$$Z_{G=D} = Z_E + \rho \int_1^{\Lambda_2} \cot \omega(P_{DE})d\lambda_2. \tag{28}$$

Finally we have:

$$Z_B = Z_C + \Lambda_1 l_o - \Lambda_1 \rho \int_1^{\Lambda_2} \frac{d\lambda_2}{\lambda_1 \sin \omega(P_{AC})}. \tag{29}$$

2.2. Perfect bond between the packer and the formation

Another limiting case is when no slip exists along the rock/packer interface. In this case, we assume that any point of the packer membrane does not move any more once it has touched the formation, *i.e.*, $u_z = 0$. Up to the touch pressure, the packer behaviour is obviously the same as that in the previous case. One therefore starts in the configuration shown in Figure 2c. Z_B is now fixed but is still given by:

$$Z_B = \rho \int_1^{\Lambda_2} \cot(\omega(P_o))d\lambda_2 \tag{30}$$

The membrane configuration when one increases the pressure from P to $P + \mathrm{d}P$ is shown on Figure 2d. Let us first analyse the bottom part of the packer. Let us assume we know the shape of the membrane at a net pressure P, and try to find the shape at $P + \mathrm{d}P$, satisfying the perfect bond condition along BE_1. The corresponding situation in the reference body is:

$$D'E_1'(P) = -\rho \int_1^{\Lambda_2} \frac{\mathrm{d}\lambda_2}{\lambda_1 \sin[\omega(P)]} \tag{31}$$

and

$$D'E_1'(P + \mathrm{d}P) = -\rho \int_1^{\Lambda_2} \frac{\mathrm{d}\lambda_2}{\lambda_1 \sin[\omega(P + \mathrm{d}P)]}; \tag{32}$$

therefore:

$$\begin{aligned} \mathrm{d}E_1'(P) &= D'E_1'(P + \mathrm{d}P) - D'E_1'(P) \\ &= -\rho \int_1^{\Lambda_2} \frac{\mathrm{d}\lambda_2}{\lambda_1} \left(\frac{1}{\sin \omega[(P + \mathrm{d}P)]} - \frac{1}{\sin[\omega(P)]} \right); \end{aligned} \tag{33}$$

hence

$$\frac{\mathrm{d}E_1'(P)}{\mathrm{d}P} = -\rho \int_1^{\Lambda_2} \frac{\mathrm{d}\lambda_2}{\lambda_1} \frac{\mathrm{d}}{\mathrm{d}P} \frac{1}{\sin[\omega(P)]} = \rho \int_1^{\Lambda_2} \frac{\mathrm{d}\lambda_2}{\lambda_1} \left(\frac{\cos[\omega(P)]}{\sin^2[\omega(P)]} \right) \frac{\mathrm{d}\omega(P)}{\mathrm{d}P}. \tag{34}$$

Integrating from touch pressure P_o to current net pressure P, we have:

$$\int_{P_o}^{P} \mathrm{d}E_1'(P) = -\rho \int_1^{\Lambda_2} \frac{\mathrm{d}\lambda_2}{\lambda_1} \left(\frac{1}{\sin[\omega(P)]} - \frac{1}{\sin[\omega(P_o)]} \right). \tag{35}$$

Hence

$$B'E_1' = -\rho \int_1^{\Lambda_2} \frac{\mathrm{d}\lambda_2}{\lambda_1} \left(\frac{1}{\sin[\omega(P_{D_1E_1})]} - \frac{1}{\sin[\omega(P_o)]} \right). \tag{36}$$

Recognising that

$$\rho \int_1^{\Lambda_2} \frac{\mathrm{d}\lambda_2}{\lambda_1 \sin[\omega(P_o)]} = l_o \tag{37}$$

we observe that

$$B'E_1' = l_o - \rho \int_1^{\Lambda_2} \frac{\mathrm{d}\lambda_2}{\lambda_1 \sin[\omega(P_{D_1E_1})]} \tag{38}$$

and

$$BE_1 = \Lambda_1(B'E'), \tag{39}$$

which gives for Z_{E_1}:

$$Z_{E_1} = Z_B + \Lambda_1 l_o - \Lambda_1 \rho \int_1^{\Lambda_2} \frac{\mathrm{d}\lambda_2}{\lambda_1 \sin[\omega(P_{D_1E_1})]}. \tag{40}$$

Similarly:

$$D_1'E_1' = -\rho \int_1^{\Lambda_2} \cot[\omega(P_{D_1E_1)}]\, \mathrm{d}\lambda_2, \tag{41}$$

which gives for Z_{D_1}:

$$Z_{D_1} = Z_B + \Lambda_1 l_o - \Lambda_1 \rho \int_1^{\Lambda_2} \frac{\mathrm{d}\lambda_2}{\lambda_1} \frac{1}{\sin[\omega(P_{D_1E_1})]} + \rho \int_1^{\Lambda_2} \cot[\omega(P_{D_1E_1})]\, \mathrm{d}\lambda_2. \tag{42}$$

Any point G between D and E is given by:

$$Z_G(\lambda_2^*) = Z_{E_1} + \rho \int_{\lambda_2^*}^{\Lambda_2} \cot[\omega(P_{DE})]\, \mathrm{d}\lambda_2 \tag{43}$$

with $\lambda_2^* = r/\rho$.

Note that, although the derivation is different, these equations yield, within a constant due to the different position of point B, the very same shape as for the perfect slip case. In fact, along the portion where the membrane is in contact with the wellbore wall, the membrane ignores the behaviour of the rock/packer interface once the maximum expansion ratio Λ_2 is fixed. This is a consequence of the hypothesis that the cords are inextensible.

For the top part, two limiting cases can be considered: either A and B are both fixed, or B is fixed and A is free to move. Experiments show that the real behaviour lies somewhere in between these two limiting cases.

If one considers that A and B are fixed, one has:

$$Z_{C_1} = \rho \int_1^{\Lambda_2} \cot[\omega(P_{AC})]\, \mathrm{d}\lambda_2. \tag{44}$$

Any point F between A and C is given by

$$Z_F(\lambda_2^*) = \rho \int_1^{\lambda_2^*} \cot[\omega(P_{AC})]\, \mathrm{d}\lambda_2 \tag{45}$$

with $\lambda_2^* = r/\rho$. However,

$$A'C_1' = \rho \int_1^{\Lambda_2} \frac{\mathrm{d}\lambda_2}{\lambda_1 \sin[\omega(P_{AC_1})]} \tag{46}$$

and

$$A'B' = \rho \int_1^{\Lambda_2} \frac{\mathrm{d}\lambda_2}{\lambda_1 \sin[\omega(P_o)]} = l_o, \tag{47}$$

hence $C_1'B' = A'B' - A'C_1'$ can not satisfy the constraint $\Lambda_1(C_1'B') = C_1B$. This either means that the packer loses its integrity as it sticks to the wall, or that the cords have to extend to satisfy this condition, which is not allowed within the restrictions of this model.

If one considers that the top part of the packer is free to move, the top part of the packer will be pulled down to keep the integrity of the packer. Then, following a similar reasoning to that for the bottom part of the packer, one finds:

$$Z_{C_1} = Z_B - \Lambda_1 l_o + \Lambda_1 \rho \int_1^{\Lambda_2} \frac{\mathrm{d}\lambda_2}{\lambda_1 \sin[\omega(P_{A_1C_1})]}, \tag{48}$$

$$Z_A = Z_{C_1} - \rho \int_1^{\Lambda_2} \cot[\omega(P_{A_1C_1})] \mathrm{d}\lambda_2, \tag{49}$$

$$Z_F(\lambda_2^*) = Z_{C_1} - \rho \int_{\lambda_2^*}^{\Lambda_2} \cot[\omega(P_{A_1C_1})]\ \mathrm{d}\lambda_2 \tag{50}$$

with $\lambda_2^* = r/\rho$. Note that, as for the bottom part of the packer, this yields the same shape, within a constant, as for the perfect slip case.

3. Determination of the pressure acting on the formation

At each point in the contact zone, the pressure acting on the formation P_f is equal to the current pressure in the packer P_k minus the pressure that is taken by the membrane. The pressure taken by the membrane actually corresponds to the net pressure acting across the membrane when it did touch the wall at that point for the first time in the reference coordinate system. P_f therefore varies from well pressure at the end points of the interval, to a maximum of $P_k - P_o$ at the initial membrane midpoint.

3.1. Perfect slip between the rock and the packer

Following the same notation as in Figure 2b, we can write the pressure acting on the formation P_f across the contact zone. For any point J belonging to the top contact half - length CB of the membrane:

$$P_f(z_J) = P_k - P, \tag{51}$$

where P satisfies the following integral equation:

$$z_B - z_J = \Lambda_1 \left(l_o - \rho \int_1^{\Lambda_2} \frac{\mathrm{d}\lambda_2}{\lambda_1 \sin[\omega(P)]} \right). \tag{52}$$

Also

$$P_f(z_C) = P_k - (P_k - P_1) = P_1, \tag{53}$$
$$P_f(z_B) = P_k - P_o. \tag{54}$$

Similarly, for any point K belonging to the bottom contact half-length BE of the membrane:

$$P_f(z_K) = P_k - P, \tag{55}$$

where P satisfies the following integral equation:

$$z_K - z_B = \Lambda_1 \left(l_o - \rho \int_1^{\Lambda_2} \frac{\mathrm{d}\lambda_2}{\lambda_1 \sin[\omega(P)]} \right). \tag{56}$$

Also

$$P_f(z_B) = P_k - P_o, \tag{57}$$
$$P_f(z_D) = P_k - (P_k - P_2) = P_2. \tag{58}$$

3.2. PERFECT BOND BETWEEN THE ROCK AND THE PACKER

Following the same notation as in Figure 2c, we can write the pressure acting on the formation P_f across the contact zone. For any point G belonging to the bottom contact half-length BE_1 of the membrane:

$$P_f(z_G) = P_k - P, \tag{59}$$

where P satisfies the following integral equation:

$$z_G - z_B = \Lambda_1 \left(l_o - \rho \int_1^{\Lambda_2} \frac{\mathrm{d}\lambda_2}{\lambda_1 \sin[\omega(P)]} \right), \tag{60}$$

which has the same form as equation (56). Note that z_B is, however, different. We also have

$$P_f(z_B) = P_k - P_o, \tag{61}$$

$$P_f(z_{E_1}) = P_2. \tag{62}$$

Similarly, for any point F belonging to the top contact half-length BC_1 of the membrane:

$$P_f(z_F) = P_k - P, \tag{63}$$

where P satisfies one of the two following integral equations:

– if it is considered that the top part of the packer cannot move:

$$z_F = \rho \int_1^{\Lambda_2} \cot[\omega(P)]\, \mathrm{d}\lambda_2; \tag{64}$$

– if it is considered that the top part of the packer can be pulled down:

$$z_B - z_F = \Lambda_1 \left(l_o - \rho \int_1^{\Lambda_2} \frac{\mathrm{d}\lambda_2}{\lambda_1 \sin[\omega(P)]} \right). \tag{65}$$

We also have

$$P_f(z_{C_1}) = P_1, \tag{66}$$

$$P_f(z_B) = P_k - P_o. \tag{67}$$

4. Results

In this section we first analyze the pressure applied to the rock by a single packer and a straddle packer arrangement, then we analyze the influence of the pressure imposed by the packer on the wellbore wall and its effect on the state of stress in the rock.

4.1. SINGLE PACKER

Results are presented for a 5″-diameter packer and a maximum inflation ratio of 1·8. The initial length of the membrane was 1 m, its initial thickness of 1 cm, and its strain energy density parameters as in (1). The initial distance between two adjacent cords was 5 mm. These are, to the best of our knowledge, typical parameters for a packer element. For a single packer arrangement, the same value is assigned to the pressure above and below the packer. This means that the net pressure is the same for the top and the bottom part of the packer.

The shape of the deformed membrane is presented in Figure 3 for different values of the net pressure inside the packer: touch pressure, 0·1 MPa, 1 MPa, 5 MPa and 10 MPa. Slat packers

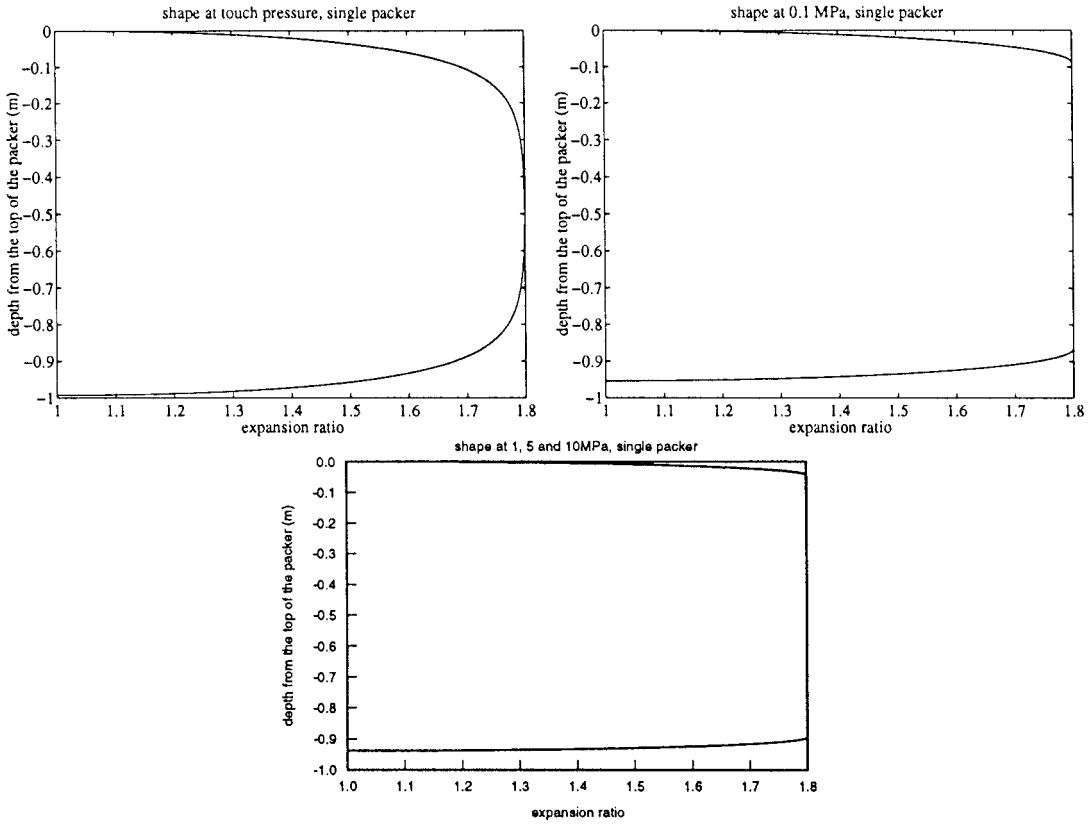

Figure 3. Single packer arrangement, one family of cords: deformed shape of the membrane for various net pressures across the membrane.

have been considered here, namely that the initial angle between the families of cords is zero (there is only one family of longitudinal cords). It is also worth noting that the changes in the packer shape are minimal once the net pressure has reached 1 MPa: hence we have plotted the shapes for 1 MPa, 5 MPa and 10 MPa in the same figure. Most of the changes in shape occur close to the net pressure, which is very low for this case (about 0·075 MPa).

In order to test the influence of the initial angle between the cords, the deformed shape of the membrane is presented in Figure 4 for an initial angle of 10 degrees, for touch pressure and 5 MPa. Yet again, the packer seems to lock into a specific shape once the net pressure reaches 1 MPa, hence the presentation of the profile for 5 MPa only. The only difference with the previous computations is that the packer is now able to get slightly shorter whilst expanding and that the touch pressure is slightly higher (of the order of 0·079 MPa).

A profile of pressure acting on the formation is presented in Figure 5 for a single family of cords and a net pressure of 0·1, 1, 5 and 10 MPa. As the touch pressure is low compared to the inflation pressure, the pressure is nearly constant along the contact zone and is close to the net pressure. For comparison, the pressure profile for a net pressure of 5 MPa is presented in Figure 6 when the angle between the two families of reinforcing cords is equal to 10 degrees. The shape of the profile is essentially similar to that presented in the previous figure.

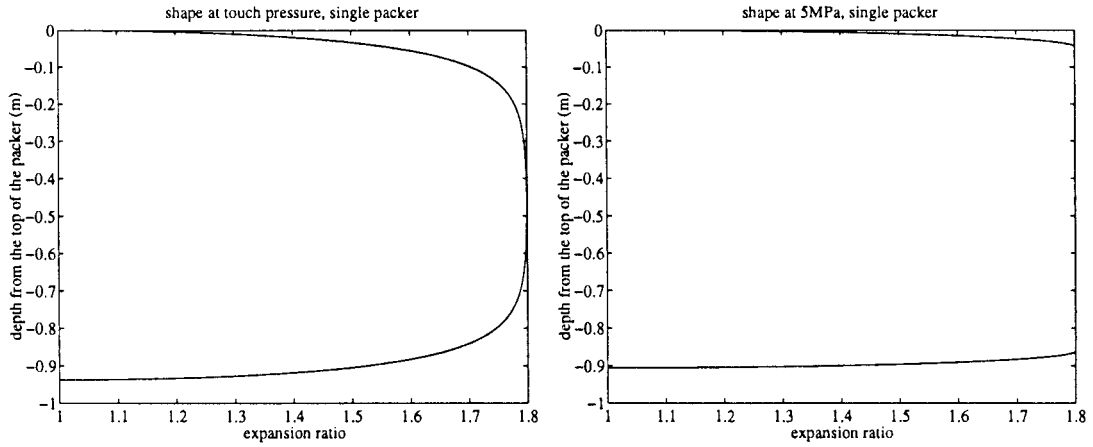

Figure 4. Single packer arrangement, two families of cords ($\alpha = 10°$): deformed shape of the membrane for various net pressures across the membrane.

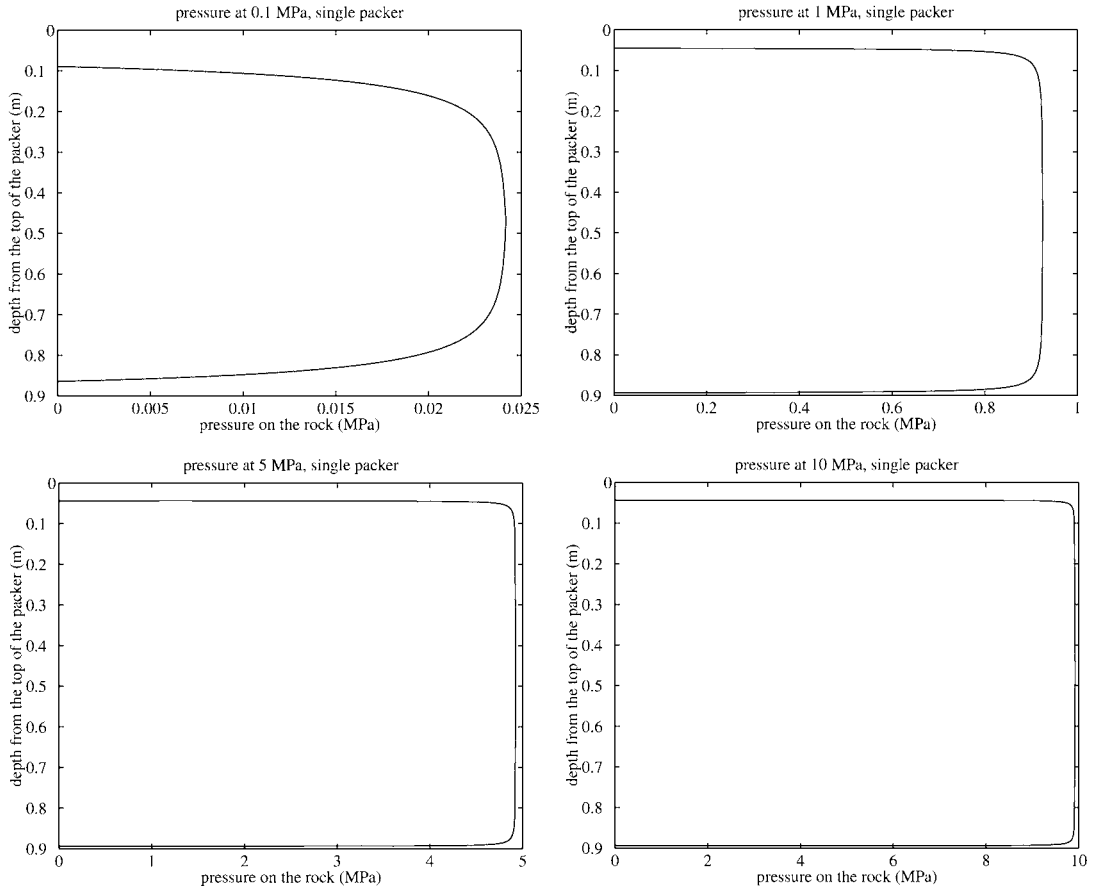

Figure 5. Single packer arrangement, one family of cords: profile of pressure acting on the wellbore for various net pressures across the membrane.

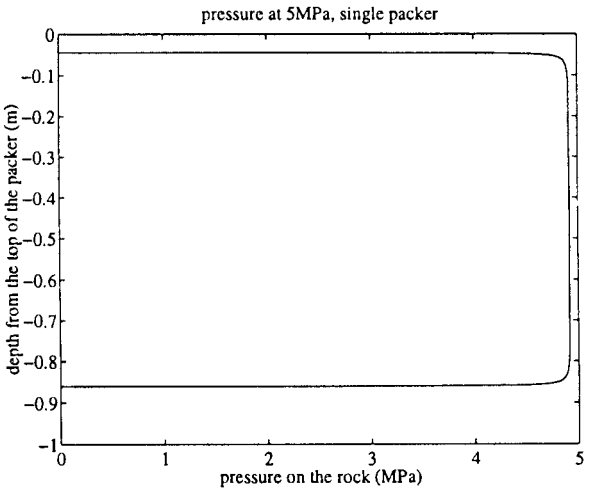

Figure 6. Single packer arrangement, two families of cords ($\alpha = 10°$): profile of pressure acting on the wellbore for a net pressure of 5 MPa across the membrane.

4.2. STRADDLE PACKER ARRANGEMENT

For a straddle packer arrangement, a different value is assigned to the pressure above and below the packers. For the top of the top packer and the bottom of the bottom packer, the external pressure is equal to the hydrostatic pressure. For the bottom of the top packer and the top of the bottom packer, the external pressure is equal to the interval pressure, typically 1 MPa lower than the internal pressure in the packers. This only arises when sealing is achieved, *i.e.*, when the net pressure is above touch pressure. The characteristics of the packers and the wellbore dimension are similar to that of the previous section.

The shapes of the deformed membrane, for both the top and bottom packers and for 5 MPa and 10 MPa net pressures across the membrane, are presented in Figure 7. All four shapes are almost identical, hence are presented in a single figure. As the angle between the families of reinforcing cords does not have much influence here, the case for slat packers has only been considered here. The shape at touch pressure has not been reproduced as it is similar to that presented in Figure 3. A profile of pressure acting on the formation is presented in Figure 8 for a single family of cords and a net pressure of 5 and 10 MPa. The pressure is nearly constant across most of the contact area and equal for both the top and the bottom packers. Note that the pressure acting on the formation is 4 and 9 MPa in the interval, for the the 5 MPa and 10 MPa net pressure cases respectively.

4.3. STRESS FIELD GENERATED BY A SINGLE PACKER INTO THE ROCK. FINITE--ELEMENT ANALYSIS

The results shown in the previous subsection demonstrate that the pressure applied on the wellbore wall by the packer, is nearly uniform. Such an almost constant presssure distribution is a result of the assumption of a rigid wellbore. Nevertheless, we now have to compute the stresses developed in the elastic rock, due to packer inflation. We expect that the radial displacement on the wellore will be very small, such that the profile of constant pressure is not altered. In an attempt to justify the constant pressure argument, we calculated the radial displacement u at the midpoint of the packer/rock interface, using the semi-analytic method

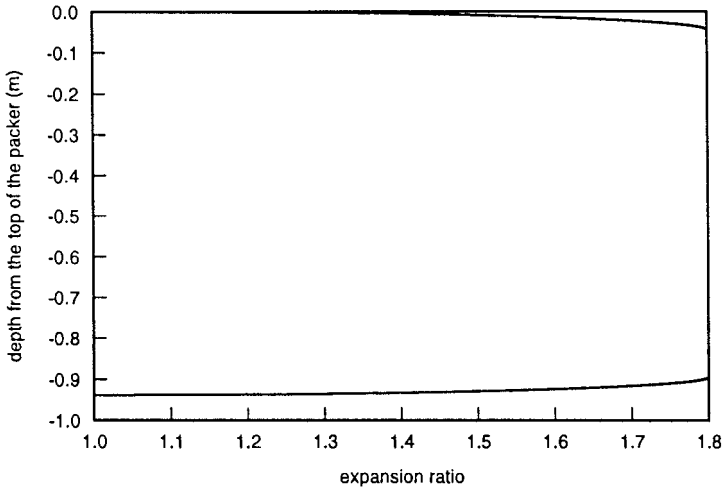

Figure 7. Straddle packer arrangement, one family of cords: deformed shape of the membrane for 5 MPa and 10 MPa net pressures across the membrane for both top and bottom packers.

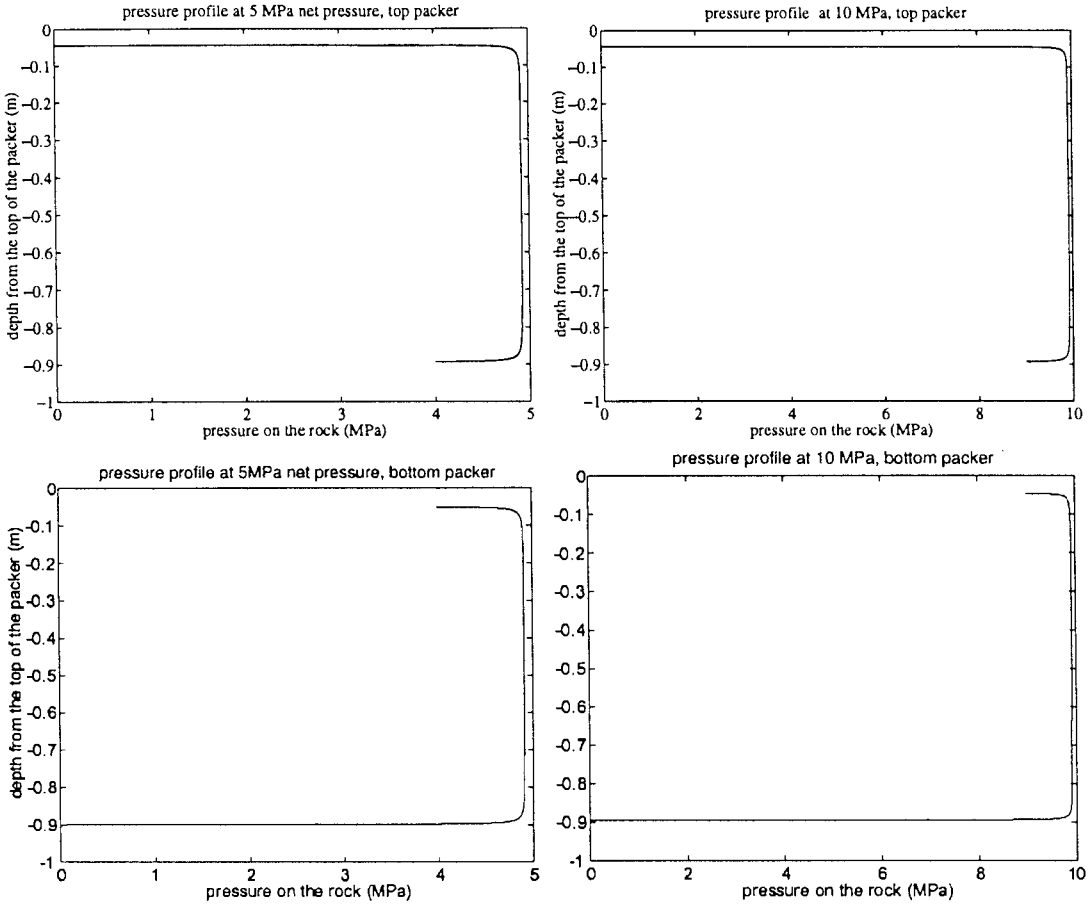

Figure 8. Straddle packer arrangement, one family of cords: profile of pressure acting on the wellbore for various net pressures across the membrane.

Table 1. The radial displacement at the midpoint of the packer/wellbore interface

	$E = 50$ GPa	$E = 20$ GPa	$E = 10$ GPa
Pure slip	$2{\cdot}6 \times 10^{-5}$m	$6{\cdot}7 \times 10^{-5}$m	$1{\cdot}3 \times 10^{-4}$m
Pure bond	$2{\cdot}6 \times 10^{-5}$m	$6{\cdot}6 \times 10^{-5}$m	$1{\cdot}3 \times 10^{-4}$m

presented in Appendix B. In that example a single packer with one family of cords is inflated at 10 MPa in a 9 inch diameter wellbore; the resulting contact length is 0·84 m; the elasticity modulus of the rock is either 10 GPa, or 20 GPa or 50 GPa and its Poisson's ratio is 0·2. Results appear in Table 1.

Note that values of the radial displacement at other points (different from the midpoint of the contact length) along the packer/wellbore interface, are smaller than the ones presented in Table 1.

Next we assumed that the wellbore radius is increased by 6.6×10^{-5}m, *i.e.*, the value indicated in Table (1) for a rock with Young's modulus $E = 20$ GPa. We calculated the touch pressure for the displaced wellbore, which turned out to be in relative error of order 10^{-4}, with the touch pressure for the rigid wellbore. Hence the small wellbore radial diplacement does not actually alter the touch pressure. Since the determination of the touch pressure from (8), is the starting point for finding the shape of the membrane and the pressure on the rock, the latter should not change compared to the one found by assuming a rigid wellbore. We have therefore assumed that the pressure is constant over the rock packer/interface, in order to analyze the state of stress in the rock.

The following axisymmetric problem has been considered: the formation is infinite, linear elastic, with a circular cylindrical hole in the middle; no stress is applied to the formation (known analytic solutions which provide the stress field around the wellbore in presence of far-field stresses can be superposed if required); no pressure is acting on the hole boundary apart from a finite strip where a pressure P_f is acting. We only consider the influence of a single packer. The problem of the state of stress imposed by a straddle packer arrangement can also be obtained by superposition.

Both pure slip and pure bond cases have been considered. For the pure slip condition, zero shear stress $\tau_{rz} = 0$ along the entire wellbore wall is considered. For the perfect bond condition, zero axial displacement $u_z = 0$ along the strip over which the non-zero pressure acts, is considered. These two cases are two extremes as some shear stress will be left even if the contact between the packer and the wellbore wall is lubricated by mud cake. Furthermore, it is difficult to believe that the packer membrane will be stiff enough to prevent any vertical movement of the formation during loading. Anyhow, these provide bounds on the actual stress acting on the formation.

As an example, the following analysis has been run using the finite element package ANSYS 5.5.1: a packer is inflated at 10 MPa in a 9 inch diameter wellbore; the resulting contact length is 0·84 m; the elasticity modulus of the rock is 20GPa and its Poisson's ratio is 0·2. Due to the axial symmetry about the z axis and due to symmetry with respect to the $z = 0$ plane, only a quarter of the actual geometry is considered. In Figure 9, a part of the discretisation close to the contact region, is shown. Note that the Y axis in ANSYS corresponds to the z axis of our notation. The arrows on the left indicate the applied pressure along the contact

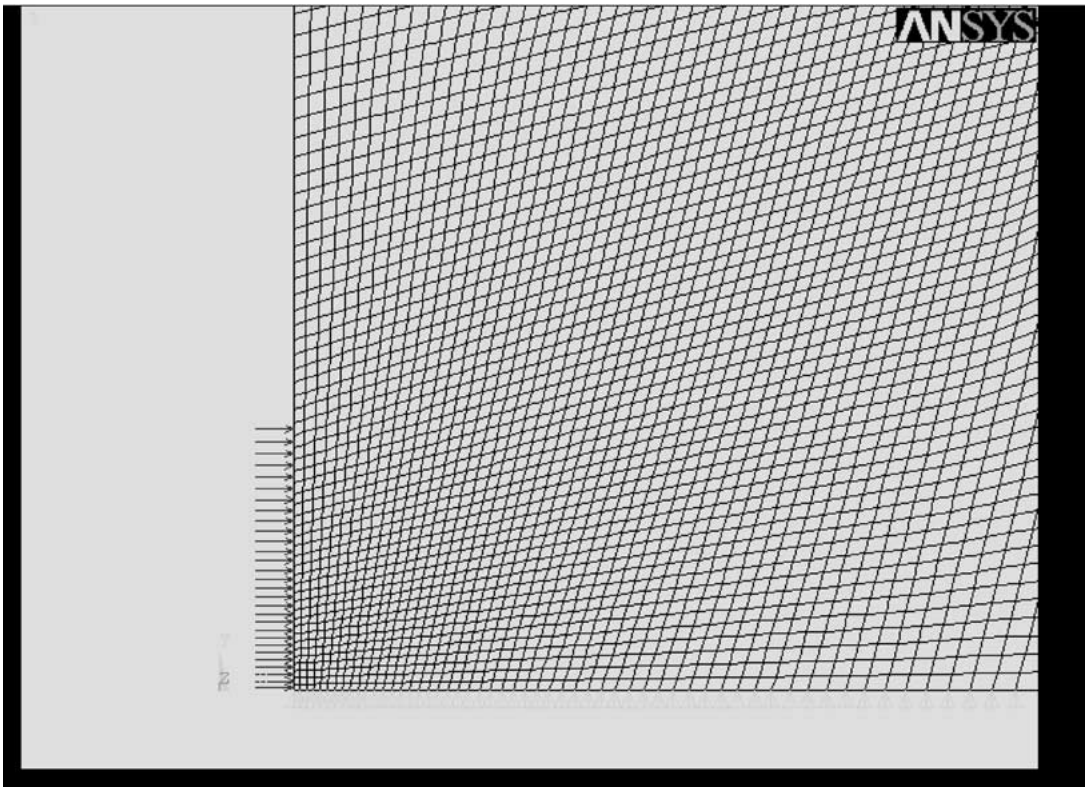

Figure 9. The finite element discretisation in the vicinity of the contact region.

half length and the triangles along the bottom side indicate rolling frictionless hinges. A rectangular area with dimensions 25 times bigger than the contact length is discretised. Hinges are imposed along the two far-field sides of this rectangular area (these sides do not appear in Figure 9 and are 50 contact half-lengths far away from the pressure loading).

Vertical profiles of the axial stress σ_{zz} in the rock, are shown in Figures 10 (perfect slip) and 11 (perfect bond). The locations where the maximum and the minimum axial stresses are developed, are indicated by MX and MN, respectively. The corresponding values are assigned to variables SMX and SMN on the right side of the graphs.

Tensile axial stresses develop for both geometries. They are maximum close to the end point of the packer, just outside the contact region, for both the perfect slip and the perfect bond case. Tensile axial stresses are however small compared to the radial and tangential stresses that develop in the formation.

Figures 5 and 5 present vertical profiles of radial stress σ_{rr}, tangential stress $\sigma_{\theta\theta}$ and axial stress σ_{zz} measured one tenth of a wellbore radius away from the wellbore. Results are obtained from the finite element model (dashed line) as well as from a semi-analytic approach (solid line), that is outlined in Appendix B. The stresses are normalised with respect to the absolute value of the pressure $|P_f|$ applied on the rock . The axial distance is normalised with respect to the contact half length. Results from both methods are almost identical.

The value for σ_{zz} is, for both cases, significantly smaller than the two other stresses. However, the maximum positive σ_{zz} for the perfect slip case is almost three times larger than σ_{zz} for the perfect bond case.

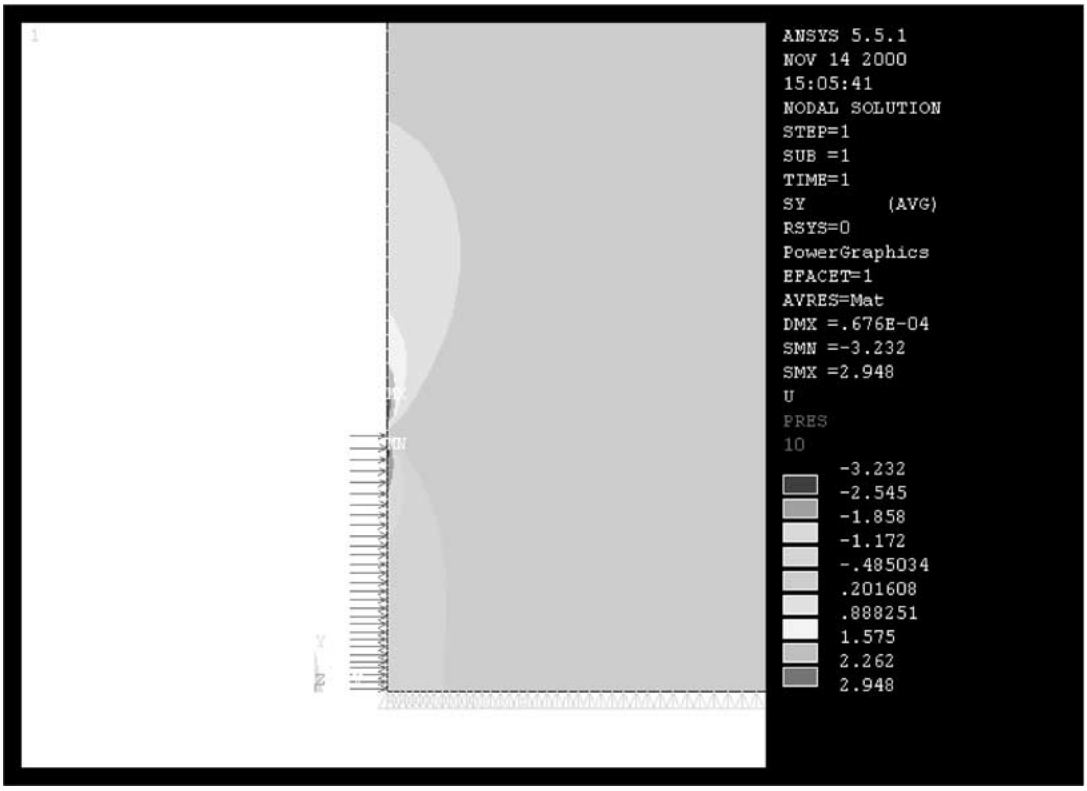

Figure 10. Contours of the resulting axial stress σ_{zz} in the formation: perfect slip between the packer and the formation.

Another important result, which is a consequence of the small value of the touch pressure, is the confirmation that the tangential stress $\sigma_{\theta\theta}$ at the wellbore wall will be close to packer pressure. During a micro-hydraulic fracturing test, the packer pressure is higher than the interval pressure to ensure packer sealing. This means that the tangential stress $\sigma_{\theta\theta}$ will be higher at packer level than at interval level. The risk of crack initiation at packer level exists, unless the fracture has been initiated in the interval prior to micro-hydraulic fracture testing, using the sleeve fracturing technique for example [5].

5. Conclusions

With this model and the range of parameters taken as typical for an MRPA packer element, touch pressures are small compared to typical inflation pressures reached during a stress test. This is in accordance with what is observed in the field and has several important consequences.

- a significant contact area between the packer and the wellbore wall is already developed even at low differential pressures;
- for interpretation purposes, assuming that a uniform pressure is applied to the rock along the contact length is a good approximation; the value of this uniform pressure is close to the packer inflation pressure;
- although the straddle packer arrangement considered here is not symmetrical, very little difference appears between the behaviour of the top and the bottom packer;

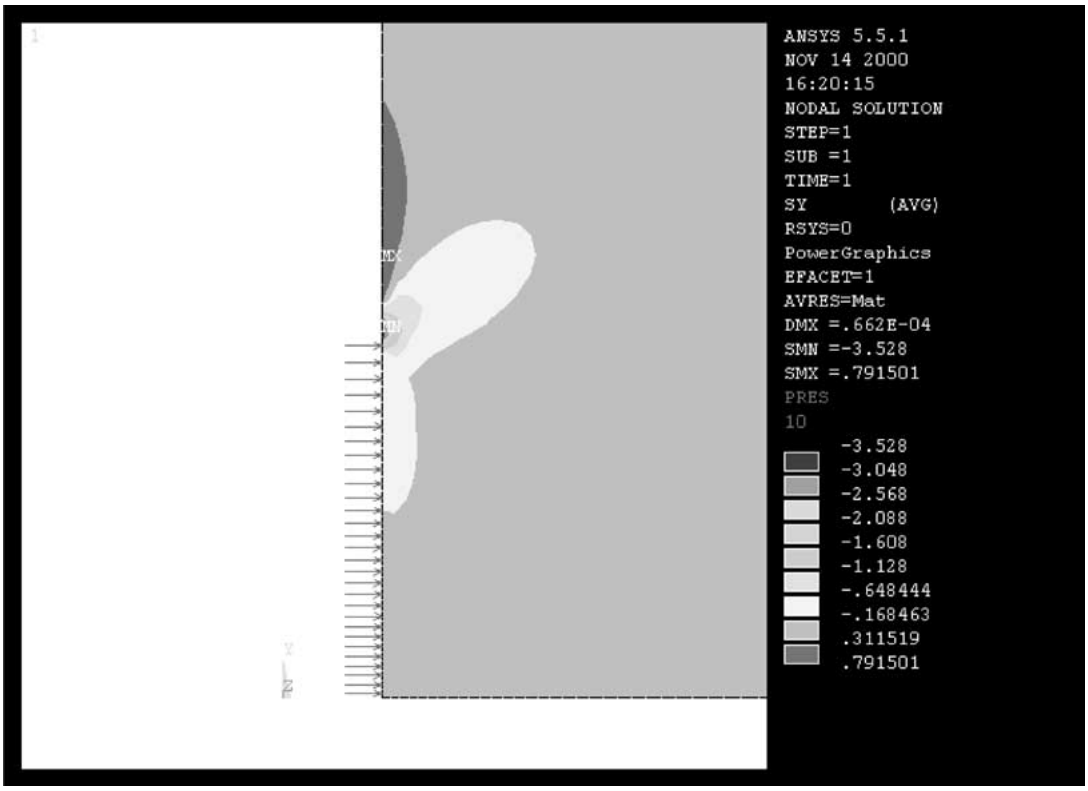

Figure 11. Contours of the resulting axial stress σ_{zz} in the formation: perfect bond between the packer and the formation.

– the tangential stress $\sigma_{\theta\theta}$ at wellbore wall (see Figures 12 and 13) is close to packer pressure; during micro-hydraulic fracturing testing, the risk exists that the hydraulic fracture may be initiated at packer level; this provides a justification of the use of sleeve fracturing prior to hydraulic fracturing to ensure proper location of the fracture;

These conclusions could change if a packer is developed for which the touch pressure is much higher.

As far as the model for the packer itself is concerned, no real difference is observed between a perfect slip or a perfect bond between the packer and the wellbore wall. A difference exists, however, for the stresses that develop in the formation because of packer inflation. For both cases, tensile axial stresses develop at packer ends but are much smaller than the pressure applied to the formation. The tangential tensile stresses that develop at packer level, however, are for both cases of the order of magnitude of the pressure applied to the formation. This implies that, during a sleeve fracturing operation, creation of an axial fracture along the entire contact length is much more likely than creation of a transverse fracture.

Appendix A. Nomenclature

(O, r, θ, z) – cylindrical coordinate system; (O, ρ, θ, η) – cylindrical coordinate system; A, B, C, D, E, F, G, J, K – points on the deformed membrane; A', B', C', D', E', F', G', J', K' – corresponding points on the undeformed membrane; $2h_0$ – initial membrane thickness (l); I_1, I_2 – strain invariants; $2l_o$ – initial membrane length (l); P – net pressure across the mem-

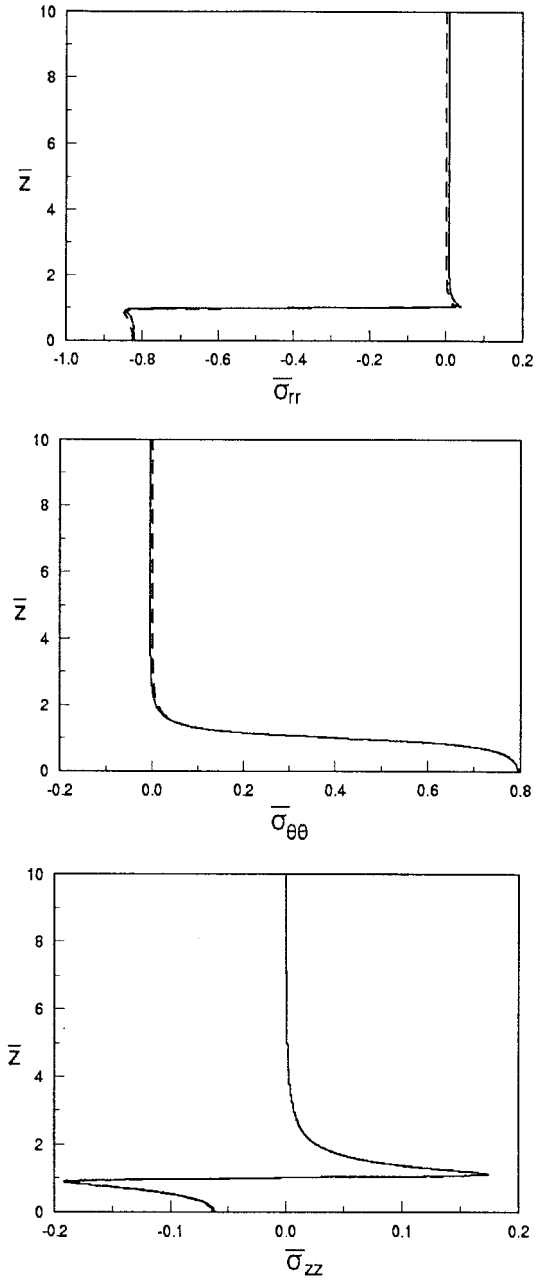

Figure 12. Vertical profiles of normalised radial stress, tangential stress and axial stress taken 0·1 wellbore radius away from the wellbore: perfect slip case. Semi-analytic (solid line) and finite element (dashed line) approach.

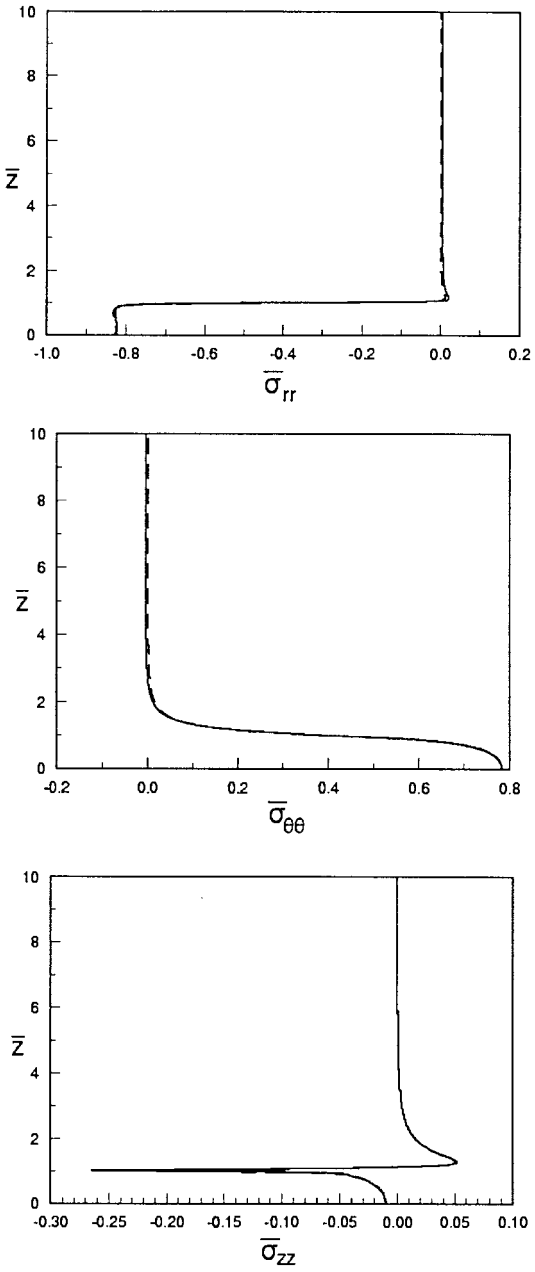

Figure 13. Vertical profiles of normalised radial stress, tangential stress and axial stress taken 0·1 wellbore radius away from the wellbore: perfect bond case. Semi-analytic (solid line) and finite element (dashed line) approach.

brane ($ml^{-1}t^{-2}$) ; P_0 – constant net pressure across the membrane; P_1, P_2 – total pressure above and below the packer; P_f – pressure acting on the formation; P_h – hydrostatic pressure in the well; P_k – pressure in the packer; P_o – touch pressure; R_w – wellbore radius (l); W – strain energy ($ml^{-1}t^{-2}$); α – initial angle between the cords and the cylinder generator; ξ – curvilinear coordinate along the deformed meridian (l); λ_1 – meridian extension ratio; λ_2 – radial extension ratio; Λ_1 – maximum λ_1; Λ_2 – maximum λ_2 *i.e.* packer expansion ratio; ω – angle between the tangent of the deformed meridian and the axis of symmetry;

Appendix B

A semi-analytic solution for the stress field in the rock, generated by a single packer, is presented here. The stresses and displacements for the axisymmetric problem of a circular cylindrical hole in an infinite medium, are given in [6, pp. 383–385] by

$$u = \left[\frac{3m-4}{m} f(x) - x f'(x) - g'(x)\right] \cos\beta\zeta, \tag{B1}$$

$$w = \left[x f(x) + g(x)\right] \beta \sin\beta\zeta, \tag{B2}$$

$$\frac{R_w}{2G}\sigma_{rr} = \left[\frac{3m-2}{m} f'(x) - \left(\beta^2 x + \frac{m-2}{mx}\right) f(x) + \frac{g'(x)}{x} - \beta^2 g(x)\right] \cos\beta\zeta, \tag{B3}$$

$$\frac{R_w}{2G}\sigma_{\theta\theta} = \left[\frac{3m-2}{mx} f(x) - \frac{m-2}{m} f'(x) - \frac{g'(x)}{x}\right] \cos\beta\zeta, \tag{B4}$$

$$\frac{R_w}{2G}\sigma_{zz} = \left[\left(\frac{2}{mx} + \beta^2 x\right) f(x) + \frac{2f'(x)}{m} + \beta^2 g(x)\right] \cos\beta\zeta, \tag{B5}$$

$$\frac{R_w}{2G}\tau_{\rho z} = \left[x f'(x) - \frac{m-2}{m} f(x) + g'(x)\right] \beta \sin\beta\zeta \tag{B6}$$

where u is the radial displacement, w is the axial displacement, σ_{rr} is the radial stress, $\sigma_{\theta\theta}$ is the hoop stress, σ_{zz} is the axial stress, τ_{rz} is the shear stress, R_w is the wellbore radius, G is the shear modulus of the rock, $m = 2(\lambda + G)/\lambda$ with $\lambda = \nu E/(1+\nu)\,(1-2\nu)$. E is the Young's modulus and ν is the Poisson's ratio. $x = r/R_w$ is the normalised radial distance, $\zeta = z/R_w$ is the normalised axial distance. Also

$$f(x) = C_2 K_1(\beta x), \tag{B7}$$

$$g(x) = D_2 K_0(\beta x) \tag{B8}$$

with $K_1(\beta x)$, $K_0(\beta x)$ being the modified Bessel functions. C_2 and D_2 are constants to be determined so that the boundary conditions on the wellbore are satisfied. β is a variable, which we will integrate over, later on.

We consider again the case of a single (axially symmetric) packer, lying symmetrically with respect to the $z = 0$ plane. It's contact half-length is a. For the perfect slip case, we have on the wellbore

$$\sigma_{rr} = P_f \text{ for } 0 \le z < a, \tag{B9}$$

$$\sigma_{rr} = 0 \text{ for } z > a, \tag{B10}$$

$$\tau_{rz} = 0 \text{ for } z \ge 0. \tag{B11}$$

If we write these stresses from (B3) and (B6), as cosine and sine transforms

$$\sigma_{rr} = \left(\frac{2}{\pi}\right)^{1/2} \int_0^\infty F(\beta) \cos \beta\zeta \, d\beta, \tag{B12}$$

$$\tau_{rz} = \left(\frac{2}{\pi}\right)^{1/2} \int_0^\infty G_1(\beta) \sin \beta\zeta \, d\beta \tag{B13}$$

with

$$\left(\frac{2}{\pi}\right)^{1/2} \frac{R_w}{2G} F(\beta) = \lim_{x\to 1} \left[\frac{3m-2}{m} f'(x) - \left(\beta^2 + \frac{m-2}{m}\right) f(1) + g'(x) - \beta^2 g(1) \right], \tag{B14}$$

$$\left(\frac{2}{\pi}\right)^{1/2} \frac{R_w}{2G} G_1(\beta) = \lim_{x\to 1} \left[f'(x) - \frac{m-2}{m} f(1) + g'(x) \right] \beta, \tag{B15}$$

we require that

$$F(\beta) = \left(\frac{2}{\pi}\right)^{1/2} P_f \frac{\sin(a'\beta)}{\beta}, \tag{B16}$$

$$G_1(\beta) = 0, \tag{B17}$$

where $a' = a/R_w$ is the normalised contact half-length. From (B14) and (B15), taking into account (B7) and (B8), we can find C_2 and D_2 in terms of β. Then, by integrating the right-hand sides of relations (B1–B6), over β from 0 to ∞, all stresses and displacements can be evaluated at any point (x, ζ) in the rock.

For the perfect bond case, we have to satisfy the following boundary conditions on the wellbore

$$\sigma_{rr} = P_f \quad \text{for} \quad 0 \le z < a, \tag{B18}$$

$$w = 0 \quad \text{for} \quad 0 \le z < a, \tag{B19}$$

$$\tau_{rz} = 0 \quad \text{for} \quad z > a, \tag{B20}$$

$$\sigma_{rr} = 0 \quad \text{for} \quad z > a. \tag{B21}$$

From (B13), we write the shear stress $g_1(\zeta)$ on the wellbore ($x = 1$) as a sine transform,

$$g_1(\zeta) = \left(\frac{2}{\pi}\right)^{1/2} \int_0^\infty G_1(\beta) \sin \beta\zeta \, d\beta \tag{B22}$$

with $G_1(\beta)$ given from (B15). When it is also assumed that the shear stress can be expressed as

$$g_1(\zeta) = \delta(\zeta - \alpha') \tag{B23}$$

on the wellbore ($\delta(\zeta - \alpha')$ is the Dirac delta function, $\alpha' = \frac{\alpha}{R_w}$ and $0 \le \alpha < a$), from (B22) and (B23) we find

$$G_1(\beta) = \left(\frac{2}{\pi}\right)^{1/2} \sin(\beta\alpha'). \tag{B24}$$

Writing the shear stress within the contact region $0 \leq \zeta < a'$, in terms of an unknown distribution $T(\alpha')$ as

$$g_1(\zeta) = \int_0^{a'} T(\alpha')\delta(\zeta - \alpha')\, d\alpha'. \tag{B25}$$

and taking into account (B24), we eventually find

$$G_1(\beta) = \left(\frac{2}{\pi}\right)^{1/2} \int_0^{a'} T(\alpha') \sin(\beta\alpha')\, d\alpha'. \tag{B26}$$

Again equations (B14) and (B15) are solved for C_2 and D_2. $F(\beta)$ is given from (B16) but $G_1(\beta)$ is now given from (B26). Thus C_2 and D_2 are found in terms of the unknown distribution $T(\alpha')$. Their expressions are then inserted in (B2), whose right-hand side is written as an integral over β from 0 to ∞. $T(\alpha')$ is then evaluated from (B19), by solving an integral equation numerically. Finally, C_2 and D_2 are explicitly determined and stresses and displacements can be found at any point in the rock, from (B1–B6), by integrating the right hand sides over β from 0 to ∞.

For the numerical evaluation of the Fourier integrals we use the routine `dftint` from [7, pp. 584–591].

References

1. M. Thiercelin, R. Plumb, J. Desroches, P. Bixenman, J. Jonas and W. Davie, A New Wireline Tool for in-situ Stress Measurements. In: *Proceedings SPE Joint Rocky Mountain Regional and Low Permeability Reservoirs Symposium.* Denver (1993) pp. 635–646.
2. A. D. Kydoniefs, Finite axisymmetric deformations of an initially cylindrical membrane reinforced with inextensible cords. *Quart. J. Mech. Appl. Math.* 23 (1970) 481–488.
3. C. Atkinson and B. Peltier, The finite deformation of a reinforced packer, membrane theory. *J. Eng. Math.* 27 (1993) 443–454.
4. A. M. Priest, Inflatable Packer Development; Progress Report for May 1991. MERL report, Materials Engineering research Laboratory Ltd (May 1991).
5. M. Thiercelin, J. Desroches and A. Kurkjian, Open Hole Stress Test in Shales. In: *Proceedings of the Eurock'94 symposium: Rock Mechanics in Petroleum Engineering*, Delft, Netherlands (1994) pp. 921–928.
6. A. I. Luré, *Three Dimensional Problems of the Theory of Elasticity.* New York: Interscience (1964) 493 pp.
7. W. H. Press , S. A. Teukolsky, W. T. Vetterling, B. P. Flannery, *Numerical Recipes in C.* Cambridge: Cambridge University Press (1994) 994 pp.